NANO LETTERS

2007
Vol. 7, No. 6
1697−1700

Plasmonic Crystal Demultiplexer and Multiports

A. Drezet,* Daniel Koller, Andreas Hohenau, Alfred Leitner, Franz R. Aussenegg, and Joachim R. Krenn

Institute of Physics and Erwin Schrödinger Institute for Nanoscale Research, Karl-Franzens-University, Universitätsplatz 5, 8010 Graz, Austria

Received March 23, 2007; Revised Manuscript Received May 2, 2007

ABSTRACT

We report the realization of two-dimensional optical wavelength demultiplexers and multiports for surface plasmons polaritons (SPPs) based on plasmonic crystals, i.e., photonic crystals for SPPs. These SPP elements are built up of lithographically fabricated gold nanostructures on gold thin films. We show by direct imaging of laterally confined SPP beams in the visible spectral range by leakage radiation microscopy that SPPs of different wavelengths are efficiently rerouted into different directions. In addition we demonstrate the generation of three output SPP beams from one input beam.

Artificially built periodic optical structures in dielectric and metallic media have generated considerable interest due to their potential for optical device miniaturization.[1−4] In this context plasmonics, i.e., optics based on surface plasmon polaritons (SPPs),[3] offers new exciting prospects. SPPs are hybrid light/electron surface waves at the interface between a dielectric and a metal[5] and as such hold the potential for two-dimensional (2D) optical functionality. Indeed, SPP elements as mirrors, splitters, and interferometers have been recently demonstrated.[6−10] However, for plasmonics to qualify at the information technology level requires necessarily the realization of wavelength division (demultiplexing) which constitutes a fundamental ingredient of optical communication. In the following we experimentally demonstrate 2D SPP demultiplexing in the visible spectral range by using photonic crystals for SPPs (plasmonic crystals). In addition, we demonstrate that plasmonic crystal are capable of realizing integrated linear multiports which could constitute building blocks of analog or quantum optical computing.

The choice of 2D plasmonic crystals to achieve our goal is motivated by the fact that such metal-based structures can generate huge optical band gaps.[11] Indeed, complete SPP confinement (i.e., an all-angle optical band gap) has been demonstrated[12] which opens up a venue for SPP-based waveguiding.[13] Simpler geometries as 1D plasmonic band gap structures (Bragg mirrors or gratings) are already well mastered, typical SPP Bragg reflectors being built from periodically arranged lines of nanoscale metal protrusions or indentations on a metal film.[6,7] Bragg diffraction occurs when the in-plane wave vector $\mathbf{k}_0$ of the incoming SPP wave can pick up a momentum $G = \pm p2\pi e/d$. G is a reciprocal vector of the Bragg lattice oriented along the periodicity direction of the mirror, d is the lattice period, and p is an integer. The diffracted wave vector must consequently fulfill

$$\mathbf{k}_d = \mathbf{k}_0 + \mathbf{G} \tag{1}$$

In addition, energy conservation imposes the condition $|\mathbf{k}_d| = |\mathbf{k}_0|$ and as a consequence Bragg reflection occurs only for specific angles and wavelengths. This opens a possibility for spectral demultiplexing if we put different Bragg mirrors 1, 2, ... in series such that for each mirror eq 1 is satisfied at different SPP wavelengths λ_1, λ_2, ... For practical reasons, however, we do not use this configuration here due to the short SPP propagation length $L_{SPP} < 50$ μm in the visible spectral range. We propose rather a compact solution in which two Bragg mirrors optimized for two different wavelengths are superimposed. Indeed, if nanoscale protrusions (or indentations) are positioned at the intersection points of two sets of Bragg lines with different orientations built to reflect respectively the wavelengths λ_1 and λ_2, one obtains a 2D plasmonic crystal presenting optical band gaps around these wavelengths (Figure 1a,b).

To demonstrate this approach we have investigated a plasmonic crystal demultiplexer optimized for the two SPP wavelengths $\lambda_1 \simeq 784$ nm and $\lambda_2 \simeq 730$ nm which correspond to laser wavelengths of 800 and 750 nm, respectively. This and the samples discussed in the following were fabricated by standard electron-beam lithography and lift-off[14] on 50 nm thick gold thin films. We fabricated rectangular 2D lattices made of gold protrusions (200 nm diameter, 50 nm height); see Figure 1a. As sketched in Figure 1b we expect under such conditions that incoming SPP waves

* Corresponding author. E-mail: aurelien.drezet@uni-graz.at.

10.1021/nl070682p CCC: $37.00
Published on Web 05/15/2007

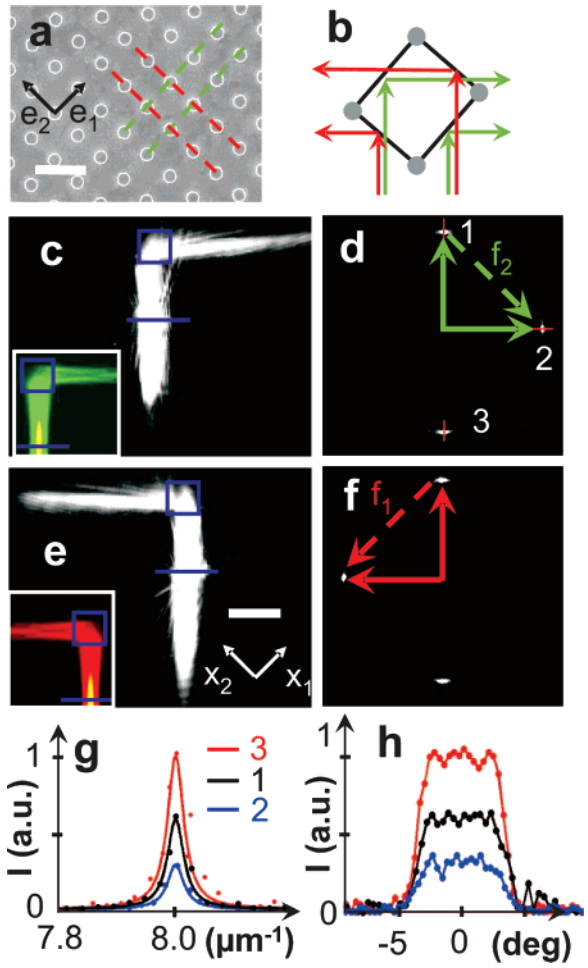

Figure 1. Plasmonic crystal demultiplexer. (a) SEM image of the crystal lattice built using electron beam lithography and made of gold protrusions (200 nm diameter, 50 nm height) deposited on a 50 nm thick gold film. ($\mathbf{e}_1$, $\mathbf{e}_2$) is the primitive lattice basis of the crystal, and the dashed lines show the two sets of Bragg lines corresponding to SPP wavelengths $\lambda_1 = 784$ nm (red) and $\lambda_2 = 730$ nm (green). The scale bar is 600 nm. (b) Sketch indicating SPP Bragg reflections for both wavelengths. (c, e) Direct space LRM images for wavelengths λ_2 and λ_1, respectively. The launching ridge and the plasmonic crystal are indicated by the blue line and the rectangle, respectively. The insets show the according simulations. (d, f) Fourier space images corresponding to panels c and e, respectively. The features 1, 2, and 3 are discussed in the text, the continuous arrows indicate the momenta of incident and reflected SPPs, and the dashed arrow represents the momentum transfer $\mathbf{f}_i$ ($i = 1, 2$) from the Bragg mirror. (g) Radial cross-cuts from panel d through 1, 2, and 3 (cross-cuts are done along the short red lines in panel d). The red, black, and blue curves correspond to Lorentzian fits for 3, 1, and 2, respectively (data points are shown with the same color). (h) Angular cross-cuts from panel d through 1, 2, and 3 along the circumference of the ring with radius $|k_{SPP}'|$ (k_{SPP}' is the real part of the wavevector associated with SPP propagating on a flat interface).[10] Colors correspond to those in panel g.

with wavelengths λ_1 and λ_2 are reflected in two opposite directions. This is indeed what is observed experimentally (compare parts c and e of Figure 1) using leakage radiation microscopy (LRM) which is based on the conversion of SPP waves to propagating light.[8,15,16]

To understand more precisely this effect, we must apply eq 1 considering the reciprocal vector $\mathbf{G} = p_1\mathbf{f}_1 + p_2\mathbf{f}_2$. The reciprocal lattice basis $\mathbf{f}_i$ ($i = 1, 2$) is connected to the primitive lattice vector basis $\mathbf{e}_i$ (see Figure 1a) by $\mathbf{f}_i = -2\pi/d_i^2\mathbf{e}_i$, where d_i values are the lattice periods $|\mathbf{e}_i| = d_i$. Values of $d_1 = \lambda_1/2^{1/2} = 554$ nm and $d_2 = \lambda_2/2^{1/2} = 516$ nm were chosen in order to realize 45° Bragg reflection. An incident SPP impinging on the crystal in the vertical direction [+1,+1] (see Figure 1a) is thus expected to be reflected to the right (i.e., the [+1,−1] direction, see Figure 1b) or to the left (i. e., the [−1,+1] direction, see Figure 1b) depending on the SPP wavelength λ_2 or λ_1, respectively. SPPs are launched by focusing a laser beam onto a gold ridge[6] and propagate subsequently in the directions [±1,±1], as seen in parts c and e of Figure 1 which show the LRM images for the SPP wavelengths λ_2 and λ_1. We observe that the SPP propagating in the direction [+1,+1] is efficiently reflected upon interaction with the plasmonic crystal as expected, i.e., to the right for λ_2 and to the left for λ_1 (Figure 1c,e).

Being a far-field optical method LRM enables the imaging and direct quantitative analysis of SPPs in both direct and Fourier space.[10,15] The Fourier image (i.e., momentum maps) corresponding to Figure 1c (Figure 1e) is shown in Figure 1d (Figure 1f) and reveals three distinct spots. The spots labeled 1 and 3 correspond to the SPPs propagating in the [+1,+1] and [−1,−1] directions, respectively, while the spot labeled 2 corresponds to the reflected SPP (Figure 1d). Due to energy conservation, all three spots (1−3) must be located on a same Ewald circle, as found in the experiment. The transfer of momentum (i.e., $\mathbf{f}_i$ at the SPP wavelength λ_i) is directly evident from the images as plotted by the dashed arrows in parts d and f of Figure 1 while incident and reflected SPPs are represented by the continuous arrows.

Furthermore, these data allow the strightforward quantitative analysis of the plasmonic crystal efficiency. For this purpose, we have to take into account the exponential damping of the SPP intensity along the SPP propagation direction. In quantitative terms, the intensities of the three spots 1−3 in parts d and f of Figure 1 are related by the expressions $I_2 = \mathrm{Re}^{-r/L_{SPP}}I_3$ and $I_1 = (1 - (1 - T)\mathrm{e}^{-r/L_{SPP}})I_3$, where R and T are the reflection and transmission coefficients of the plasmonic crystal and $r = 32$ μm is the distance separating the SPP launch ridge from the plasmonic crystal. On the basis of cross-cuts trough the spots 1−3 to retrieve quantitative information from the images (see Figure 1g), we deduced $R \simeq 80\%$ and $T \simeq 5\%$ for the SPP wavelength λ_1.[10] This implies losses $S = 1 - T - R$ of around 20% which we attribute to out-of-plane scattering. The radial shape of the observed SPP peaks (see Figure 1g) can be theoretically reproduced by using a Lorentzian fit. This is in agreement with previous studies[10,17] showing that the full width at half-maximum of such peaks are a direct measure of $1/L_{SPP}$. We found here $L_{SPP} = 30$ μm, which is in good agreement with the measurement of the exponential SPP damping in direct space (not shown). Angular cross-cuts of the SPP peaks (see Figure 1h) show that the angular divergence is conserved when going from 1 to 3. The same analysis for the SPP wavelength λ_2 yields $R \simeq 70\%$, $T \simeq 10\%$, and $S \simeq 30\%$.

To corroborate our results we simulated the interaction of a SPP beam with the plasmonic crystal by using a 2D dipolar

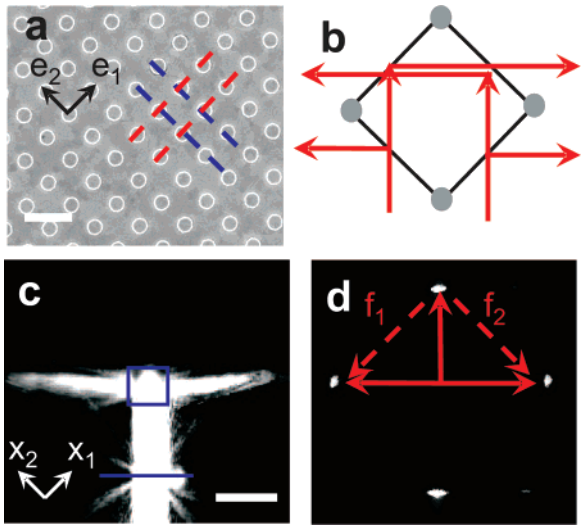

Figure 2. Plasmonic crystal splitter. (a) SEM image, ($\mathbf{e}_1$, $\mathbf{e}_2$) is the primitive lattice basis of the crystal and the dashed lines show the two sets of Bragg lines corresponding to a SPP wavelength $\lambda_2 = 730$ nm. The scale bar is 600 nm. (b) Sketch indicating SPP Bragg reflection directions. (c) Direct space LRM image. The launching ridge and the plasmonic crystal are indicated by the blue line and the rectangle, respectively. (d) Fourier space image corresponding to panel c. The scale bar is 30 μm for c. The continuous arrows indicate the momenta of incident and reflected SPPs and the dashed arrows represent the momentum transfer $\mathbf{f}_i$ ($i = 1, 2$) from the Bragg mirror.

model.[9] While interparticle coupling was neglected in our model (i.e., we worked in the limit of the first Born approximation) qualitative agreement with the experimental observations for the two considered wavelengths is obtained; see the insets in Figure 1c,e.

We now turn to the special case $\lambda_1 = \lambda_2$ (and thus a plasmonic crystal with a quadratic unit cell) which corresponds to a SPP splitter (Figure 2a,b). We studied this system for a laser wavelength of 750 nm corresponding to a SPP wavelength $\lambda_1 = \lambda_2 = 730$ nm. In the direct space LRM image in Figure 2c the splitting of the incoming SPP beam is clearly observed. In the Fourier image in Figure 2d, one observes four spots corresponding to the two counterpropagating SPPs launched from the gold ridge and to the two reflected SPP beams. This image again illustrates directly how momentum transfer operates in such a device. Quantitative analysis as above indicates that about 80% of the incoming SPP intensity is reflected equally between SPPs propagating to the right and to the left of the crystal (i.e., in the $[+1,-1]$ and $[-1,+1]$ directions, respectively). The residual part of the intensity ($S \simeq 20\%$) is again attributed to loss due to scattering.

The beam splitting and demultiplexing properties of plasmonic crystals are not restricted to two output beams. For example, choosing a triangular lattice instead of a rectangular one (Figure 3a) splits an input beam into three output beams. The triangular lattice can be thought of as resulting from the overlap of three Bragg mirrors such that the angle between the corresponding Bragg lines equals 60°. Choosing the distance d separating two adjacent parallel Bragg lines such that $d = \lambda_{SPP}/3^{1/2}$, one obtains Bragg

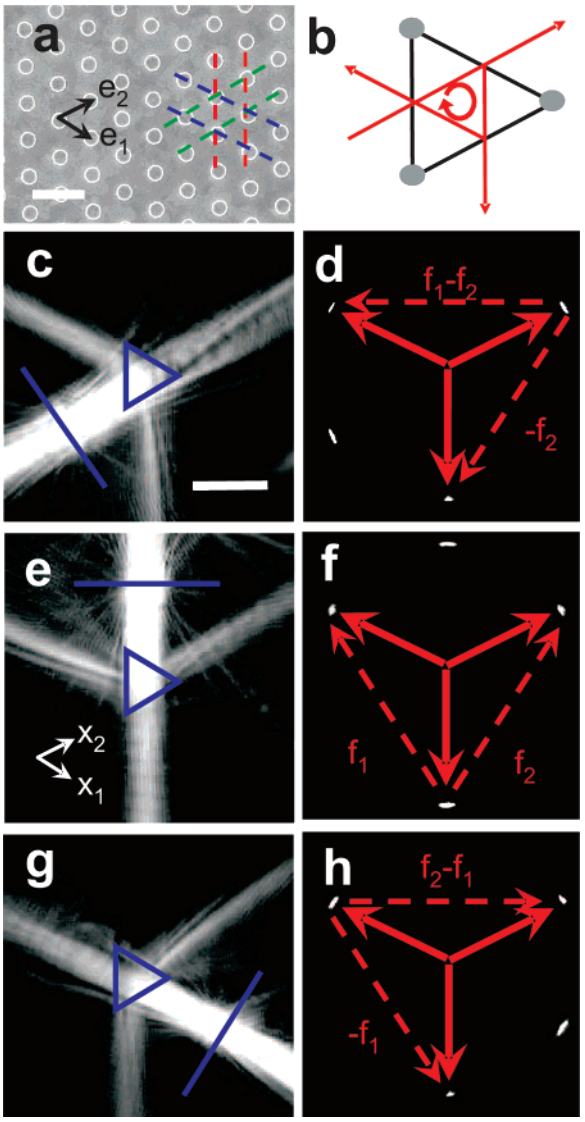

Figure 3. Plasmonic crystal tritter. (a) SEM image, ($\mathbf{e}_1$, $\mathbf{e}_2$) is the primitive lattice basis of the crystal and the dashed lines show the three sets of Bragg lines corresponding to a SPP wavelength $\lambda_2 = 730$ nm. The scale bar is 500 nm. (b) Sketch indicating SPP Bragg reflection directions. (c, e, g) Direct space LRM images. The launching ridge and the plasmonic crystal are indicated by the blue line and the triangle, respectively. The scale bar is 15 μm. (d, f, h) Fourier space images corrsponding to panels c, e, and g, respectively. The continuous arrows indicate the momenta of the incident and reflected SPPs while the dashed arrows represent the momentum transfer from the Bragg mirror.

reflection at 30° incidence angle. This corresponds to an interparticle distance in the triangular lattice of $a = 2\lambda_{SPP}/3$. Due to its symmetry such a plasmonic crystal represents a six-port device (three inputs and three outputs) that has been called "tritter" before.[18] We realized a tritter working at $\lambda_{SPP} = 730$ nm, i.e., at 750 nm laser wavelength by placing gold particles with 200 nm diameter and 70 nm height within an area enclosed by an equilateral triangle with 15 μm side length. The LRM image in Figure 3c shows that a SPP beam (incident from the lower left) is indeed split into three reflected beams. The identical results when using the two other inputs are shown in Figure 3e,g. Again, the directions of the vectors $\mathbf{f}_i$ can be taken directly from the Fourier space

images in parts d, f, and h of Figure 3 which show clearly the four spots corresponding to the incident and the three reflected SPPs. The dashed arrows correspond to a momentum transfer of $\pm\mathbf{f}_1$, $\pm\mathbf{f}_1$, or $\pm(\mathbf{f}_1 - \mathbf{f}_1)$, depending on the incident beam direction and the output beams considered (compare parts d, f, and h of Figure 3). We find that for the chosen geometry the plasmonic crystal tritter distributes 85% of the incident SPP intensity equally between the three outputs. The remaining $\simeq$15% are again attributed to scattering loss.

It should be emphasized that in the present work we deal exclusively with the coupling between 2D SPP modes with different in-plane wave vectors. The problem of coupling from a 3D propagating light mode to SPP modes was not our concern here. It has however already been demonstrated that such a coupling from 3D to 2D waves is polarization dependent[9] and can be enhanced by wavelength-dependent grating coupling (ref 4 and references therein). Plasmonic crystals could thus in principle be used as well for polarization-dependent wavelength demultiplexing from 3D light to 2D SPP waves. Finally, while all results discussed here were achieved within the visible spectral range, plasmonic crystal devices are expected to perform even better (e.g., in terms of spectral selectivity) in the infrared (telecom) spectral range due to significantly lower ohmic losses.[19] In general, SPP multiplexers, splitters, and tritters could form basic ingredients for photonic functionality where their application might be specifically appealing due to their small footprint in the range of $10 \times 10\ \mu m^2$. Furthermore, the use as building blocks for classical[20] or quantum[21] optical computing can be envisaged.

Acknowledgment. We acknowledge financial support from the EU under projects FP6 NMP4-CT-2003-505699 and FP6 2002-IST-1-507879.

References

(1) Joanopoulos, J. D.; Villeneuve, P. R.; Fan, S. Photonic crystals: putting a new twist on light. *Nature* **1997**, *386*, 143−149.
(2) Smith, D. R.; et al. Composite Medium with Simultaneously Negative Permeability and Permittivity. *Phys. Rev. Lett.* **2000**, *84*, 4184−4187.
(3) Barnes, W. L.; Dereux, A.; Ebbesen, T. W. Surface plasmon subwavlength optics. *Nature* **2003**, *424*, 824−830.
(4) Genet, C.; Ebbesen, T. W. Light in tiny holes. *Nature* **2007**, *445*, 39−46.
(5) Raether, H. *Surface Plasmons*; Springer: Berlin, 1988.
(6) Ditlbacher, H.; Krenn, J. R.; Schider, G.; Leitner, A.; Aussenegg, F. R. Two-dimensional optics with surface plasmon polaritons. *Appl. Phys. Lett.* **2002**, *81*, 1762−1764.
(7) Weeber, J.-C.; González, M. U.; Baudrion, A.-L.; Dereux, A. Surface plasmon routing along right angle bent metal strips. *Appl. Phys. Lett*. **2005**, *87*, 221101.
(8) Stepanov, A.; et al. Quantitative analysis of surface plasmon interaction with silver nanoparticles. *Opt. Lett.* **2005**, *30*, 1524−1526.
(9) Drezet, A.; et al. Surface plasmon propagation in an elliptical corral. *Appl. Phys. Lett.* **2005**, *86*, 074104.
(10) Drezet, A.; et al. How to erase surface plasmon fringes. *Appl. Phys. Lett.* **2006**, *89*, 091117.
(11) Baudrion, A. L.; et al. Influence of the filling factor on the spectral properties of plasmonic crystals. *Phys. Rev. B* **2006**, *74*, 125406.
(12) Kitson, S. C.; Barnes, W. L.; Sambles, J. R. Full Photonic Band Gap for Surface Modes in the Visible. *Phys. Rev. Lett*. **1996**, *77*, 2670−2673.
(13) Bozhevolnyi, S. I.; et al. Waveguiding in Surface Plasmon Polariton Band Gap Structures. *Phys. Rev. Lett.* **2001**, *86*, 3008−3011.
(14) Hohenau, A.; et al. Electron beam lithography, a helpful tool for nanooptics. Proceedings of MNE05, Vienna, Sept 19−22, 2005 to appear in *Microelectron. Eng*.
(15) Hecht, B.; et al. Local Excitation, Scattering, and Interference of Surface Plasmons. *Phys. Rev. Lett.* **1996**, *77*, 1889−1892.
(16) Bouhelier, A.; et al. Plasmon optics of structured silver films. *Phys. Rev. B* **2001**, *63*, 155404.
(17) Burke, J. J.; Stegeman, G. I.; Tamir, T. Surface-polariton-like waves guided by thin, lossy metal films. *Phys. Rev. B* **1986**, *33*, 5186−5201.
(18) Zukowski, M.; Zeilinger, A.; Horne, M. A. Realizable higher-dimensional two-particle entanglements via multiport beam splitters. *Phys. Rev. A* **1997**, *55*, 2564−2579.
(19) Nikolajsen, T.; et al. Polymer-based surface-plasmon-polariton stripe waveguides at telecommunication wavelengths. *Appl. Phys. Lett.* **2003**, *82*, 668−670.
(20) Saleh, B. E. A.; Teich, M. C. *Fundamentals of Photonics*; Wiley: New York, 1991.
(21) Knill, E.; Laflamme, R.; Milburn, G. J. A scheme for efficient quantum computation with linear optics. *Nature* **2001**, *409*, 46−52.

NL070682P